NANOPARTICLES

Direct proof of spontaneous translocation of lipid-covered hydrophobic nanoparticles through a phospholipid bilayer

Yachong Guo,[1] Emmanuel Terazzi,[2] Ralf Seemann,[3] Jean Baptiste Fleury,[3] Vladimir A. Baulin[1]*

Hydrophobic nanoparticles introduced into living systems may lead to increased toxicity, can activate immune cells, or can be used as nanocarriers for drug or gene delivery. It is generally accepted that small hydrophobic nanoparticles are blocked by lipid bilayers and accumulate in the bilayer core, whereas big nanoparticles can only penetrate cells through slow energy-dependent processes, such as endocytosis, lasting minutes. In contrast to expectations, we demonstrate that lipid-covered hydrophobic nanoparticles may translocate through lipid membranes by direct penetration within milliseconds. We identified the threshold size for translocation: nanoparticles with diameters smaller than 5 nm stay trapped in the bilayer, whereas those with diameters larger than 5 nm insert into the bilayer, opening pores in the bilayer. The direct proof of this size-dependent translocation was provided by an in situ observation of a single event of a nanoparticle quitting the bilayer. This was achieved with a specially designed microfluidic device combining optical fluorescence microscopy with simultaneous electrophysiological measurements. A quantitative analysis of the kinetic pathway of a single nanoparticle translocation event demonstrated that the translocation is irreversible and that the nanoparticle can translocate only once. This newly discovered one-way translocation mechanism provides numerous opportunities for biotechnological applications, ranging from targeted biomaterial elimination and/or delivery to precise and controlled trapping of nanoparticles.

INTRODUCTION

Nanoparticles (NPs) of different sizes and shapes are involved in many biomedical applications because of their abilities to insert into membranes and to internalize into cells (*1*, *2*). These applications range broadly from microscopy imaging (*3*, *4*) and cell manipulation (*5*, *6*) to diagnostics and therapeutics (*7*–*10*). Apart from numerous practical applications, NPs may also result in increased cytotoxicity (*11*). In particular, gold nanoparticles (AuNPs) may induce death of human endothelial and epithelial cells (*12*) and show increased cytotoxicity for other types of cells even at low concentrations (*11*, *13*–*15*). Cytotoxicity of AuNPs increases with concentration and depends on the size of the NPs (*15*, *16*). Hydrophobic NPs can trigger an immune response by activation of immune cells (*17*), which also increases with hydrophobicity. Because of their tiny size, hydrophobic NPs are highly mobile in aqueous solutions and present in aerosols around the planet: smoke, dust, volcanic ash, and soot. This reactivity and mobility of hydrophobic NPs raises questions about their biological effects. This generalized behavior of hydrophobic NPs can be linked to their great ability to interact with cell membranes and, in particular, to their affinity to the hydrophobic cores of membranes and bilayers. The hydrophobicity of NPs, in general, has a great effect on their binding capacity, membrane activity, and cytotoxicity (*16*, *18*–*20*). In contrast, charged NPs interact with the heads of lipids perturbing the bilayer, leading to a rich behavior including NP adsorption and bilayer rupture (*2*, *21*–*25*). The interaction of neutral hydrophobic NPs with the lipid bilayer, in turn, is rather controversial. One of the reasons for this controversy is that hydrophobic NPs need to be solubilized in the solution either by attaching ligands or by adsorbing lipids to the surface of the NPs. Depending on the molecular nature of the coating and whether it is chemically or physically bound to the NP (permanently grafted ligands, self-assembled monolayer, protein corona, or adsorbed lipids), variable interactions with lipid membranes can be found both with the lipid coating and with the core of the NP. A membrane can interact with the coating of the NP and, in the case of physically adsorbed coatings, potentially also with the core of the NPs.

Despite the large variety of coatings, chemically inert cores of neutral NPs may be characterized by only a few parameters, such as shape, size, and surface properties. This may be an indication of a universal interaction behavior of NPs with cell membranes, which, in turn, can be classified according to these parameters into groups with similar or exactly the same effect on cells.

NPs of large sizes (diameter >10 nm) usually penetrate into cells through active processes, such as different types of endocytosis (*1*, *2*, *26*, *27*). Active translocation through the cell membrane is energy-dependent, requires collective action of membrane proteins, and involves the cytoskeleton (*26*). As a result, this mechanism is slow, with a characteristic time on the order of seconds to minutes (*28*). In contrast, small solute molecules, ions, protons, and hormones (*29*, *30*), as well as fullerenes (*31*, *32*), can directly translocate through the lipid bilayer by passive diffusion. This process is energy-independent and usually takes only hundreds of nanoseconds (*29*). Thus, a huge difference in internalization time may markedly affect how cells respond to the presence of external substances, whereas one of the critical factors controlling the uptake mechanism is the size of these substances interacting with lipid membranes.

In turn, small hydrophobic NPs (diameter <10 nm) can penetrate and accumulate in bilayer cores (*33*, *34*), and it is commonly assumed that once they are trapped in the bilayer core, they cannot escape from it, which represents a potential well. Several studies, mainly based on numerical simulations, proposed strategies to enable these NPs to translocate (*35*, *36*). These strategies suggest manipulating the NP shapes (*35*) or the NP coatings by using peptides (*37*), disposable ligands (*36*), or stripped nanopatterns with a controllable symmetry (*19*, *38*–*40*). Some of these NPs could be internalized into cell membrane; however, none of them were shown to translocate experimentally through a simple phospholipid bilayer, so the translocation pathway of hydrophobic NPs remains obscure.

[1]Departament d'Enginyeria Química, Universitat Rovira i Virgili, 26 Avinguda dels Països Catalans, 43007 Tarragona, Spain. [2]Department of Inorganic and Analytical Chemistry, University of Geneva, 30 quai Ernest-Ansermet, CH-1211 Geneva 4, Switzerland. [3]Experimental Physics, Universität des Saarlandes, 66123 Saarbrücken, Germany.
*Corresponding author. Email: vladimir.baulin@urv.cat

Here, we demonstrate, both theoretically and experimentally, one-way and direct translocation of hydrophobic lipid-covered NPs through lipid bilayers (see Fig. 1). We show that NPs larger than 5 nm not only spontaneously translocate through the bilayer within milliseconds but also translocate only once because of the exchange of coating lipids between NPs and the lipid bilayer. Using the single-chain mean field (SCMF) theory (*41*–*43*), we propose a mechanism of passive translocation through lipid bilayers. By observing individual translocation events of AuNPs with 1-dodecanethiol chains (*44*, *45*) through DMPC (1,2-dimyristoyl-*sn*-glycero-3-phosphorylcholine) bilayers, we confirm the particle translocation and characterize the kinetic pathway, in agreement with our numerical predictions. The mechanism relies on spontaneous pore formation in the lipid bilayer. The observed universal interaction behavior of neutral and chemically inert NPs with the bilayer can be classified according to size and surface properties. Because of size differences, small NPs are trapped in the cores of bilayers, whereas large NPs and big clusters of NPs can translocate through lipid bilayers.

MECHANISM OF DIRECT TRANSLOCATION

The interaction between NPs of different sizes and a lipid bilayer was modeled using the SCMF theory for lipid bilayers (*43*). Previously, this method was successfully applied in studying the energy barrier during insertion of carbon nanotubes and small nano-objects into the lipid bilayer (*46*–*48*). A similar technique is used here to study the size-dependent insertion and translocation of NPs through the phospholipid bilayer. Details of the applied simulations are described in Materials and Methods.

NPs are modeled as hydrophobic spheres (*47*), with diameters ranging from 2 to 10 nm. Dodecanethiol groups grafted to the surface of NPs alter the surface chemistry and are modeled through their interaction with the phospholipid tails by an interaction parameter, ε. This interaction parameter varies from −5.0 to −7.0 kT, where a crossover between the two regimes is observed. The interaction parameter ε = −5.0 kT corresponds to a weakly hydrophobic particle and represents relatively weak attraction between the NP and the bilayer, whereas ε = −7.0 kT corresponds to a strong hydrophobic interaction, leading to a spontaneous coverage of NPs. Thus, we consider that the interaction parameter ε = −7.0 kT corresponds to lipid-coated NPs.

The different insertion regimes found in simulations are presented in Fig. 2A for different NP diameters and interaction parameters. When NPs with ε = −5.0 and −6.0 kT interact with the lipid bilayer, they insert into the core. The tails of the lipids are in direct contact with the NPs, but the interaction is not strong enough to cover the surface of the NPs with lipids and to significantly disturb the bilayer structure. For diameters <5 nm, an NP is fully integrated into the bilayer and covered by

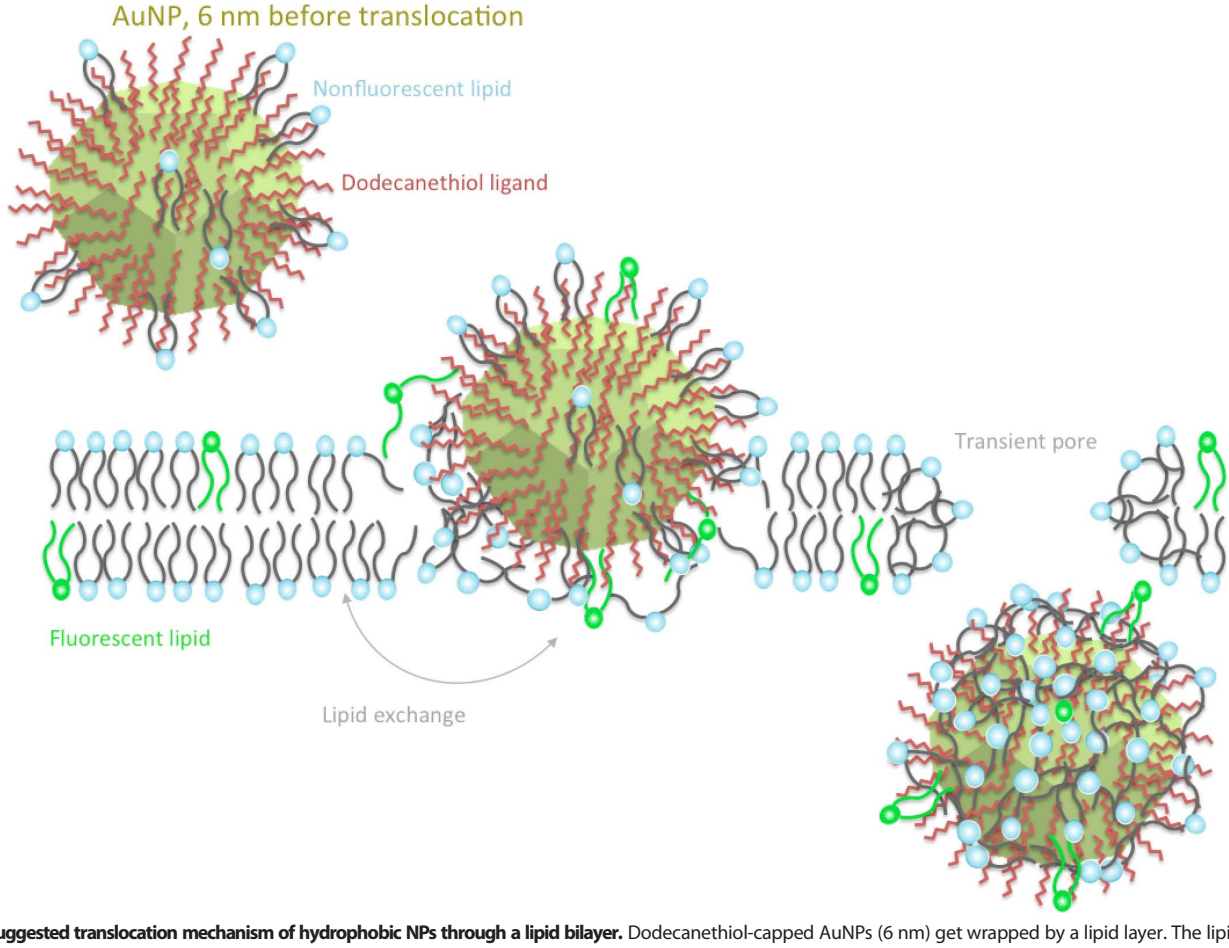

Fig. 1. Suggested translocation mechanism of hydrophobic NPs through a lipid bilayer. Dodecanethiol-capped AuNPs (6 nm) get wrapped by a lipid layer. The lipid-covered AuNPs destabilize the bilayer by generating pores and pass through the bilayer by taking away nonfluorescent and fluorescent lipids. The lipid exchange mechanism is demonstrated experimentally by starting with NPs having a nonfluorescent lipid coating, which then pick up fluorescent lipids from the bilayer upon translocation.

continuous lipid leaflets. A deformation of the lipid bilayer is observed in the vicinity of an NP because of its hydrophobic interaction with the lipid tails. For large diameters, ranging from 6.0 to 10.0 nm, an inserted NP disrupts the bilayer, creating a "hydrophobic pore" (*49*), although the tails of the lipids are closely attached to the surface of the NP. In contrast, a strong hydrophobic interaction of ε = −7.0 kT leads to a structural rearrangement of lipids in the vicinity of an NP, wrapping a lipid monolayer around the entire surface of the NP. Because of the strong binding of lipids to the NP surface in this regime, the size of the NPs determines two possible scenarios of NP-bilayer interaction: (i) small NPs, with diameters of ≤5 nm, can be fully inserted into the bilayer without significant disruption of the bilayer; (ii) large NPs, with diameters of >5 nm, do not fit into the core of the bilayer, and thus, their presence significantly alters the bilayer structure, wrapping the NP with a lipid monolayer. Because the lipids are oriented toward the surface of the NPs, there is a possibility to form a "hydrophilic pore" that is slightly larger than the radius of the NP. This scenario is similar to experimentally reported pores in a bilayer due to inserted proteins (*49*). The crossover between the two scenarios is controlled by the thickness of the bilayer, ~5 nm, which represents a characteristic length of the bilayer. This length determines the NP size when two solutions coexist simultaneously. When small NPs aggregate into clusters of larger size, they can behave similarly to NPs with larger diameters.

To quantify the interaction of NPs with a bilayer, we calculated the free energy difference per lipid molecule for the equilibrium insertion of an NP, where ΔF (*46*) is calculated with respect to the free energy of an unperturbed lipid bilayer without any NPs. The free energy difference ΔF for different interaction parameters ε is plotted in Fig. 2B as a function of NP diameter. These calculations correspond to the thermodynamic equilibrium; thus, there are no constraints on the distribution of lipids between the NP and the bilayer. Hence, the number of lipids covering the NPs is the equilibrium coverage, and the free energies correspond to the equilibrium. The more hydrophobic and larger an NP is, the more favorable is its insertion into a bilayer. A lipid bilayer thus represents a potential well for hydrophobic NPs, and one could expect that a bare hydrophobic NP, once trapped in the core of a bilayer, cannot spontaneously escape as commonly believed. We found that this is true for small NPs with diameters of <5 nm and for relatively weak attractions to lipid tails, when the topology of a lipid bilayer is not perturbed by the presence of NPs (see Fig. 2A).

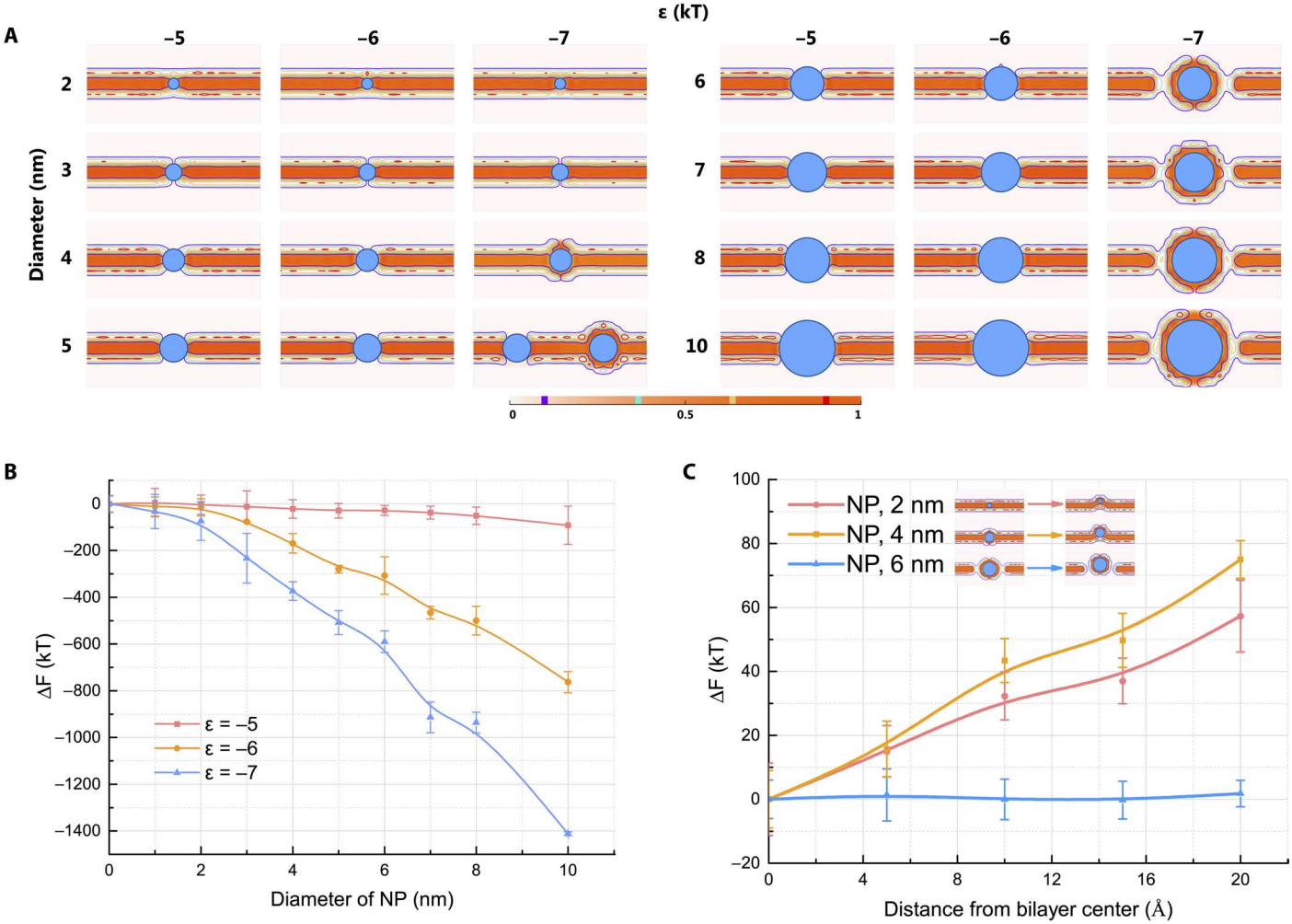

Fig. 2. Interaction of hydrophobic NPs with lipid bilayers obtained from SCMF theory. (**A**) Density profiles of lipid heads and tails around embedded NPs. The NP diameter varies between 2 nm ≤ d ≤ 10 nm, and the interaction parameter varies between −5 kT ≥ ε ≥ −7 kT. (**B**) Free energy difference ΔF as a function of the NP diameter for different interaction parameters ε. (**C**) Free energy difference ΔF as a function of the distance between the bilayer center and the core of an NP, ε = −7 kT.

However, in the case of large NPs, with diameters of >5 nm, and strong attraction, $\varepsilon = -7$ kT, the structural rearrangement of lipid tails around NPs leads to a bilayer rupture with the formation of a hydrophilic pore. In this regime, the energy gain mainly results from covering the NPs with lipids, whereas the lipid-coated NPs are only weakly connected to the lipid bilayer.

To further explore this phenomenon, we calculated the free energy cost per lipid for an NP to escape from a bilayer, ΔF, which is defined as the energy cost of moving an NP out of the center of the bilayer in a perpendicular direction. The result for $\varepsilon = -7$ kT is shown in Fig. 2C. Small NPs with diameters of 2.0 and 4.0 nm remain trapped in the bilayer and would require large energies to be extracted from the bilayer because considerable deformation and rupture of the bilayer would be needed. In contrast, there is almost no free energy barrier to extract NPs with diameters of 6 nm from the bilayer. In consequence, hydrophobic NPs $\geq$6 nm can escape from the bilayer by virtually pulling lipids out of the bilayer. The transition between a "closed" and an "open" pore may be triggered by thermal motion with relatively small free energy cost.

Having found that large and strongly hydrophobic NPs with the interaction parameter $\varepsilon = -7$ kT corresponding to NPs wrapped by lipids can leave a bilayer with a negligible cost of energy, we also explored the full translocation process across a bilayer for the interaction parameter $\varepsilon = -7$ kT, which corresponds to the experimental system of NPs coated with lipids. Then, we considered the insertion of these hydrophobic NPs into the bilayer. It turns out that the insertion of a hydrophobic lipid-coated NP into a lipid bilayer is a multistep process accompanied by the exchange of lipids between the NPs and the bilayer. The free energy difference as a function of the distance from the center of the bilayer is plotted in Fig. 3, with reference to an unperturbed bilayer and an NP in solution covered with lipids. Lipid-coated NPs approach a bilayer and touch its surface. The deformation of the lipid bilayer without rearrangements of lipids leads to an increase of the free energy and is not taken into account. However, if the NPs are brought in contact with the core of the bilayer, they can spontaneously embed into the bilayer (Fig. 3, embedding regime); this process is energetically favorable and leads to a considerable decrease of the free energy. Upon insertion, the lipid-coated NPs exchange their lipid coating with the bilayer. The transition between approaching and embedding is accompanied by a topological change in the structure of the bilayer, and thus, this transition is a first-order transition, leading to an abrupt jump from one solution to another. One can see a distinct difference between the behavior of 2- and 4-nm NPs and that of 6-nm NPs. Small NPs have only two solutions, "insertion" and "embedding" (Fig. 3, A and B), whereas 6-nm NPs have an extra regime, "escape" (blue curve in Fig. 3C). Fully embedded 6-nm NPs can rearrange lipids and form pores with almost no energy cost and leave the bilayer as previously discussed. Note that the free energy values corresponding to the escape regime in Fig. 3 (blue) are the same as those in Fig. 2C (blue). The constant energy shift between the curves is due to the choice of the reference state of the free energy of the NP embedded in the center (Fig. 2) and the unperturbed bilayer with noninteracting NPs (Fig. 3). In addition, the jumps between the solutions correspond to energy barriers, which correspond to the time of staying in metastable states.

It is noteworthy that the energy corresponding to the escape regime is ~90 kT lower than the energy of the insertion regime. This is because the initial lipid coverage of an NP due to lipid self-assembly in the solution before entering the bilayer differs significantly from that of an NP leaving the bilayer, which corresponds to the equilibrium lipid coverage. Thus, the driving force for the translocation of 6-nm NPs is the difference in the lipid surface coverage of the NPs before and after the contact with the bilayer. However, embedded NPs can escape with equal probability on both sides of the bilayer, providing symmetrical distribution of NPs around the bilayer.

EXPERIMENTAL STUDY OF A SINGLE PASSIVE TRANSLOCATION EVENT

A variant of the droplet interface bilayer technique (*50*, *51*) was used to produce a free-standing lipid membrane in a microfluidic chip (*50*, *52*, *53*). Using a volume-controlled system with syringe pumps, we injected two fingers of an aqueous phase (100 mM NaCl) face-to-face into microchannels of a cross-geometry (see Fig. 4A), which were previously filled with squalene containing a phospholipid mixture of 99% DMPC and 1% fluorescent NBD-DPPE [1,2-dipalmitoyl-*sn*-glycero-3-phosphoethanolamine-*N*-(7-nitro-2-1,3-benzoxadiazol-4-yl)] (see Materials and Methods). After a few seconds, the water-oil interface of each finger is covered with a monolayer of phospholipid molecules. Once the two liquid fingers are brought into contact, their lipid monolayers interact, forming a lipid bilayer within a short time (*51*, *52*). The bilayer is stable and can be analyzed simultaneously by optical microscopy and by electrophysiological experiments (*53*). The capacitance of the formed particle-free bilayer in this geometry is measured as $C \approx 140$ pF for a pure DMPC bilayer (see Fig. 5). Knowing the optically measured bilayer area, we can calculate the specific capacitance as $C_s \approx 4.46$ mF/m^2. From that, the corresponding bilayer thickness can be calculated as $d = \varepsilon_L \varepsilon_0 / C_s \approx 4.4$ nm, where $\varepsilon_L = 2.2$ is the dielectric constant of the lipid membrane (*51*) and $\varepsilon_0 = 8.85 \times 10^{-12}$ F/m is the vacuum permittivity. These estimates agree with literature values (*51*–*53*). Monodisperse AuNPs with diameters of 2, 4, and 6 nm are rendered hydrophobic by a covalent 1-dodecanethiol coating and are additionally covered with a DMPC monolayer to allow their dispersion in an aqueous phase (see Materials and Methods). These NPs can be added to either of the aqueous fingers.

For the first set of experiments, AuNPs are dispensed in only one of the aqueous fingers at a concentration of ≈0.1 μg/ml, which is sufficiently large for the NPs to form small clusters in solution. The other finger only contains buffer solution without any lipids or NPs. These two aqueous fingers in contact are just separated by a DMPC bilayer containing 1% of fluorescent lipids. Once the DMPC bilayer was formed and equilibrated for 20 to 30 min, AuNPs of 2 nm in diameter, covered with DMPC, were added into one of the aqueous fingers. After a few minutes, we observed a reduction in capacitance from $C \approx 140$ pF, as observed for the pure bilayer, to 127 pF for the same membrane area (see Fig. 5A). The resulting effective bilayer thickness $d \approx 4.85$ nm is larger than that of a pure lipid bilayer. The increased effective bilayer thickness indicates either insertion or accumulation of individual NPs in the bilayer. The capacitance signal is constant in time, similar to the pure bilayer, and excludes a significant exchange of NPs or their clusters with the surrounding liquid. This suggests that the particles are either partially or completely inserted into the bilayer and cannot escape (*54*). When the same experiment was repeated with 4- and 6-nm AuNPs, the capacitance is further reduced, corresponding to effective bilayer thicknesses of $d \approx 5.3$ and 5.8 nm, respectively. However, in the case of the larger NPs, the capacitance signal fluctuates on the millisecond time scale. This might result from direct contacts between the lipid bilayer and the AuNPs, which are continuously trying to insert into and to escape from the bilayer.

The capacitance measurements discussed above were complemented by optical fluorescence measurements. The DMPC-coated NPs are nonfluorescent and become visible by fluorescence microscopy only

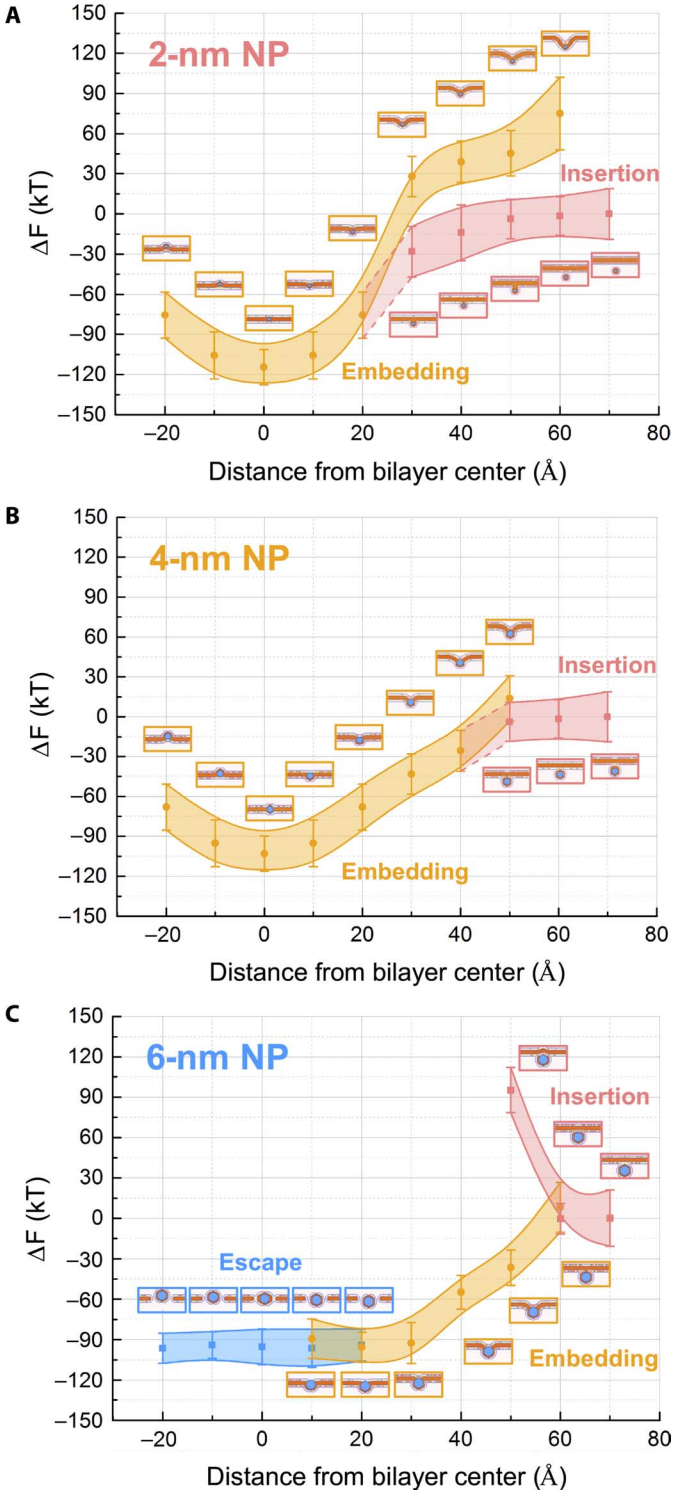

Fig. 3. Interaction regimes of trapping and translocation for hydrophobic NPs with $\varepsilon = -7.0$ kT. The interaction regimes are given by three solutions of SCMF equations for 2 nm (**A**) and 4 nm (**B**) NPs showing trapping of NPs in the bilayer and for 6-nm NPs (**C**) showing translocation of NPs. Insertion (purple): Lipid-coated NP touches the upper leaflet without structural rearrangement. Embedding (yellow): The NP fuses with the upper leaflet and exchanges its lipid coating with the bilayer. Escape (blue): The NP is wrapped by lipids, forms a pore in the bilayer, and is thus free to leave.

when taking up fluorescent lipids from the lipid bilayer. Twenty to 30 min after adding lipid-coated NPs to only one side of the bilayer, we observe a similar number of fluorescent NPs on both sides of the lipid bilayer. Conducting the same type of experiments with the nonfluorescing bilayer and NPs coated with fluorescent lipids, we observe the presence of the fluorescent lipids in the bilayer 20 to 30 min after adding the lipid-coated NPs around the bilayer (see Supplementary Materials). This shows that lipid-coated NPs can insert into the lipid bilayer and exchange lipid molecules with the bilayer. After insertion, the NPs can leave the bilayer to either side with equal probability, as predicted by the numerical results. Additional experiments with two adjacent bilayers (Supplementary Materials, Proof 3) demonstrate that NPs that translocated once across a bilayer cannot retranslocate or at least have a sufficiently lower ability to retranslocate (and remain trapped at the bilayer side to which they initially translocated). These experimental findings can be understood in line with the numerical results: while translocating, a single NP mixes its lipid coating with the bilayer upon insertion into the bilayer and extracts lipids from the bilayer upon leaving such that the lipid coating of the NP is denser after translocation than before translocation. Because this lipid wrapping after/during translocation lowers the free energy, the bilayer crossing is irreversible and can be considered as an undirected, one-way process.

From individual trajectories of NPs or clusters of NPs, the respective diffusion coefficient and the corresponding cluster or particle size can be estimated (for the conversion of diffusion coefficient to size, see the Supplementary Materials). Using this strategy, we analyze the Brownian motion of the lipid-coated NPs in the initially NP-free aqueous phase, that is, the NPs that crossed the bilayer (see Fig. 5, B to D). In the case of 2-nm NPs, no individual particles could be detected, and only the clusters of NPs could cross the bilayer. The smallest cluster size that could cross the bilayer had a diameter of 6 nm. A similar behavior was observed in the case of 4-nm NPs: individual particles could not cross the bilayer, and the smallest cluster size that could cross the bilayer had a diameter of 8 nm. The behavior observed for 6-nm NPs is remarkably different: for this particle size, individual particles could also cross the bilayer. Since smaller particles and dye molecules are unable to cross the bilayer (see the Supplementary Materials), the ability of lipid-coated particles or clusters with diameter $d \geq 6$ nm to cross the bilayer excludes spontaneous membrane poration as the governing effect. Together with the previous electrophysiological results, this demonstrates passive translocation as the mechanism that allows NPs to cross the bilayer.

To also explore the pathway of the translocation, the abovementioned experiments were repeated for 6-nm AuNPs, which were shown to cross the bilayer as individual particles. To exclude cooperative effects, we conducted the experiments at an extremely low particle concentration of 0.01 ng/ml, making clustering of NPs into aggregates very unlikely. Thus, this setup ensures the observation of a single NP translocation. Moreover, because of the resulting low frequency of translocation events, a particle translocation observed by fluorescence microscopy can be unambiguously correlated to a simultaneously measured electrophysiological signal. Figure 4C shows a single NP with a diameter of 6 nm leaving the bilayer to the initially NP-free side; the size of the NP is confirmed by the Brownian motion analysis. The corresponding membrane conductance during the translocation is presented in Fig. 6A, showing a three-step process. Starting at $t = 0$, the membrane conductance G is equal to the control value, which confirms that the membrane is impermeable to ionic charges. At $t =$ 2.5 ms, the conductance increases to $G = 1.3$ nS. At $t = 5.2$ ms (that is, 2.7 ms later), a second jump in conductance is observed at $G \approx 30$ nS.

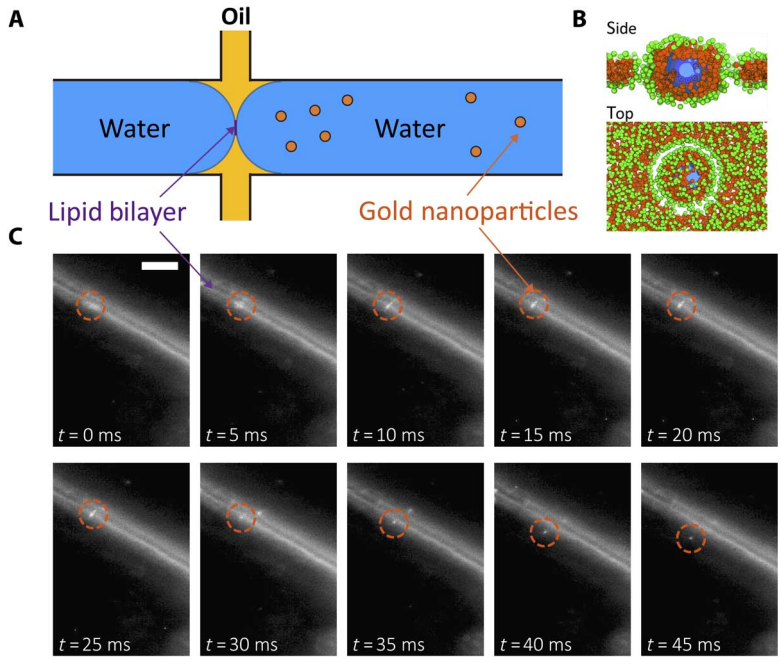

Fig. 4. Microfluidic setup. (**A**) Two aqueous fingers surrounded by squalene-lipid solution form a bilayer at their contact area. NPs can be added to the aqueous phase of either of the aqueous fingers. (**B**) Visualization of the most probable conformations of lipids around a pore formed by large hydrophobic NPs, $d = 6.0$ nm and $\varepsilon = -7$ kT, and modeled by SCMF theory. (**C**) Optical fluorescence microscopy time series demonstrating a single NP translocating through a lipid bilayer. AuNPs were added to the aqueous finger at the right. The NP leaving the bilayer (bright spot) to the initially particle-free side of the bilayer is indicated by a dashed circle. Another NP leaving the membrane to the side of the bilayer, which initially contains NPs, is visible from $t = 30$ ms.

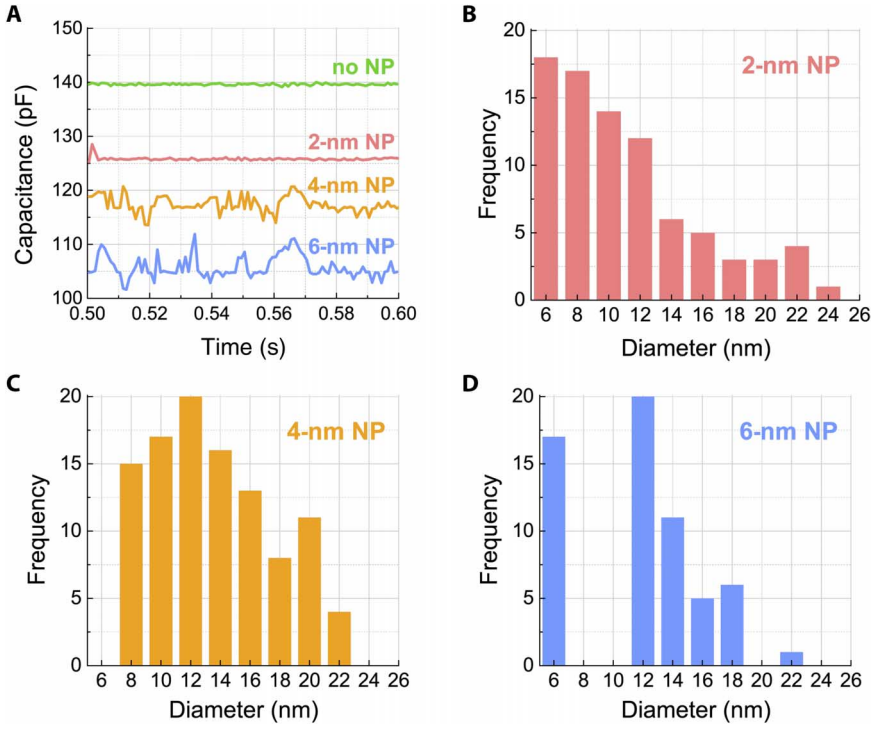

Fig. 5. Experimental interaction of NPs with the bilayer. Measurements were performed for lipid-coated AuNPs with diameters of 2 nm (pink), 4 nm (orange), and 6 nm (blue) at a concentration of $c \approx 0.1$ μg/ml. (**A**) Capacitance measurements as a function of time of a pure DMPC bilayer (green) and of a DMPC bilayer in the presence of NPs dispersed in the aqueous phase. (**B** to **D**) Size distribution of NPs that crossed the bilayer [2 nm (B), 4 nm (C), and 6 nm (D)], as analyzed from their Brownian motion. For the sake of clarity, the histograms are plotted as a function of the particle core diameter without the 1-dodecanethiol and DMPC coating.

At t = 9.3 ms (that is, another 4.1 ms later), the conductance drops down again to the control value.

Let us interpret the conductance measurements shown in Fig. 6A in view of the numerical results that describe the entire translocation event as a three-step process: insertion, embedding, and escape (see Fig. 3). The insertion and embedding should not be seen with conductance measurements because no pores are associated to these steps. However, the previous fluorescence measurements showed a lipid exchange between a lipid-coated NP and a bilayer, demonstrating the insertion and embedding steps as predicted by the numerical results. Accordingly, the first jump can be understood as the formation of a hydrophilic pore, which is the first part of the escape process. The second jump corresponds to the particle leaving the pore, whereas the return of the conductance to the control value corresponds to the pore closure.

The formation of the hydrophilic pore results in a gap size d_g between the lipid-coated NP and the bilayer and can be estimated as

$$d_g \approx \frac{Gd}{2\pi k R_{NPL}} \approx 0.1\text{nm} \quad (1)$$

where k = 1.15 S/m is the bulk electrolyte conductivity (measured for 100 mM NaCl at 30°C), $d \approx 4.4$ nm is the bilayer thickness, and $R_{NPL} \approx 6$ nm is the radius of the used NPs with a core diameter of 6 nm, functionalized with 1-dodecanethiol with a length of 1.6 nm and a DMPC monolayer coating of ≈2.5 nm (*55*). Therefore, we can suppose a lipid interdigitation with the dodecanethiol layer of ~1 nm. The obtained gap size agrees with the numerical model and is large enough to allow NPs to escape the bilayer by thermal motion. The typical lifetime of the hydrophilic pore can be considered as translocation time and was found to be on the order of a few milliseconds (see Fig. 6B). We suppose that the gap is not uniform during its lifetime, and thin lipid bridges might maintain the contact of the NP to the bilayer. This explains that the process of lipid extraction and reorganization of the bilayer is not instantaneous.

When the lipid-covered NP finally escapes the hydrophilic pore, the bilayer conductance is expected to increase massively, and the experimentally measured conductance can be used to calculate the radius of the pore

$$R_{NPL} = \sqrt{\frac{Gd}{k\pi}} \approx 6\text{nm} \quad (2)$$

This value again agrees with the coated NPs used. The lifetime of this open pore without a particle is found to be also on the order of a few milliseconds. The pore created during translocation does not lead to bilayer rupture, despite the fact that the transiently occurring pore is larger than the critical pore radius $R_c = \sigma/\Gamma \approx 1.2$ nm, calculated from the membrane free energy. The membrane rupture is likely prevented by the short pore lifetime. Similarly, there are experimental measurements demonstrating the nondestructive presence of large NP clusters in vesicles (*33*).

The translocation process is a one-way process: while translocating, a single NP extracts lipids from the bilayer such that the lipid coating of the NPs is denser after the translocation. Because this lipid wrapping and translocation process lowers the free energy, the bilayer crossing is a one-way process and the translocated NP cannot enter the bilayer again, which is confirmed experimentally in the Supplementary Materials (Proof 3).

CONCLUSIONS

In a combined numerical and experimental study using the SCMF theory and a microfluidic approach, we investigated a process of passive translocation of single hydrophobic AuNP through a lipid bilayer. For this purpose, we developed an apparatus that can monitor the translocation of a single NP and suggest the mechanism of nanotoxicity on a single-NP level. In contrast to general expectations, we demonstrate that lipid-covered hydrophobic AuNPs can not only spontaneously translocate but also translocate only once and within milliseconds.

It was found that the interaction of NPs with the lipid bilayer depends on the size of NPs. We could identify a threshold size of NP determined by the bilayer thickness as a natural lengthscale. In particular, single NPs

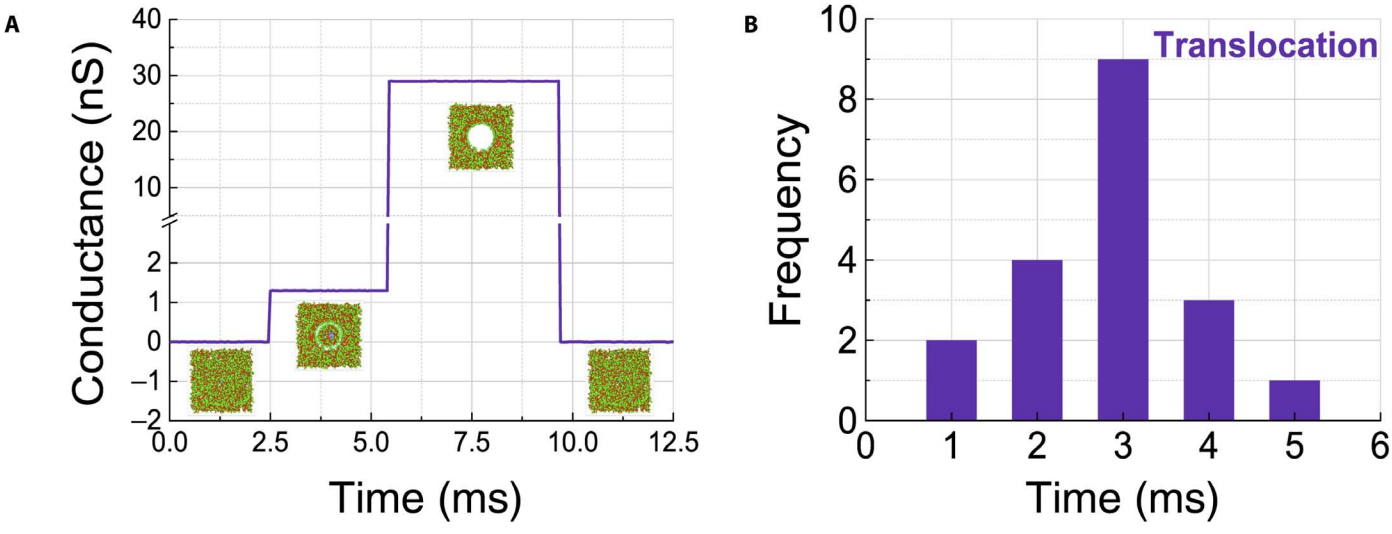

Fig. 6. Kinetic translocation pathway. (**A**) Conductance measurement during a single translocation event from a 6-nm AuNP recorded at low particle concentration of $c \approx 0.01$ ng/ml. The insets represent the different stages of the translocation pathway, as found by numerical simulation. (**B**) Translocation times measured from several individual translocation events.

with diameters $d > 5$ nm translocate through the bilayer, whereas individual NPs with diameters $d \leq 5$ nm are trapped in the bilayer. These small NPs can leave the bilayer only when forming clusters exceeding the threshold size. Other conditions and parameters, such as lipid composition and elastic and curvature energies, may additionally influence this threshold, but we expect no change in the order of magnitude.

The translocation pathway numerically predicted by the SCMF theory is confirmed by studying single translocation events with time-resolved optical fluorescence and electrophysiological measurements in our microfluidic setup. After the insertion of a hydrophobic NP into a bilayer, the lipid molecules reorganize and flip their tails toward the NP, completely wrapping the NP. This lipid-wrapped NP is only weakly bound to the lipid bilayer and forms a spontaneous pore that can open with thermal energies, enabling passive translocation of NPs. The measured lifetime of this spontaneous pore during translocation was found to be on the order of a few milliseconds, and the pore closes again without rupturing the bilayer. During the insertion process of a lipid-coated NP into the bilayer, the NP exchanges its lipid coating with the bilayer and, in turn, extracts lipid molecules from the bilayer during the translocation event, similar to the reported lipid extraction by graphene nanosheets (*56*). However, as predicted by the theoretical analysis, the coating of an NP entering the bilayer is not the same when leaving the bilayer. Because this lipid wrapping and translocation process lowers the free energy, the bilayer crossing is a one-way process, and the translocated NP cannot enter the bilayer again, which is confirmed experimentally in the Supplementary Materials (Proof 3).

The observed and described mechanism allows for the translocation of homogeneously coated NPs without the need of any nanopatterning, as reported by Verma *et al.* (*18*) and Verma and Stellacci (*19*). Furthermore, understanding this phenomenon can shed light on several biologically and environmentally relevant questions, such as dangers related to the uptake of tiny hydrophobic NPs by aquatic animals and the potential harm of NPs present in cosmetics and skin creams. The reported lipid exchange between NPs and the lipid bilayer can be used to alter cell membrane composition and delivery "to" and "from" the lipid bilayer. This mechanism provides numerous opportunities for biotechnological applications, ranging from targeted biomaterial elimination and/or precise delivery to the membrane or trapping in the cells. Specific coating of NPs opens perspectives to deliver objects such as RNA, ligands, or short biopolymers through the membrane or into the membrane.

MATERIALS AND METHODS

SCMF theory

The SCMF (*46*–*48*) can reproduce equilibrium and mechanical properties and free energies of self-assembled objects with different geometries and molecular structures. Phospholipids were modeled at a coarse-grained level within the three-bead model (*43*), which provided accurate equilibrium and mechanical properties of DMPC lipid bilayers. NPs were modeled as hard spheres fixed in the center of the bilayer. More precisely, an NP represents a spherical region in the simulation box that is not accessible for phospholipids. We assumed that the sphere could interact with hydrophobic tails of phospholipids but that the lipids could not go inside this region. The interaction parameter with NPs varies between ε values of −5.0, −6.0, and −7.0 kT, whereas the interaction range is fixed and equal to 8.1 Å. The lipid molecule was modeled as three freely jointed spherical beads of equal radius, 4.05 Å, connected by a stiff bond of 10 Å (*43*). The beads interacted through square-well potentials: between two hydrophobic beads, $\varepsilon_{TT} = -2.1$ kT with the interaction range $r = 12.15$ Å, and between one hydrophilic bead and implicit solvent, $\varepsilon_{HS} = -0.15$ kT with the interaction range $r = 12.15$ Å. The solvent molecule was considered to be of the same radius as the spherical beads. The simulation box with a size of 300 Å × 300 Å × 150 Å was divided into two-dimensional cylindrical layers around the z axis in the center of the simulation box. The conformational sampling of lipid molecules was 4,000,000 conformations.

To calculate the free energy, we assumed that the simulation box represents a part of an extensive system with an NP located inside the simulation box, where the rest of the extensive system is a continuous repetition of the NP perturbed membrane, used as a reference state for the free energy. This allowed the calculation of the free energy F of a large system from the calculation of the simulation box. It can be written as a sum of the free energy of the simulation box, F_{box}, and the free energy of the equilibrium system out of the box, F_{out}. If we assume that there is no NP inside the simulation box as a reference state, F can be denoted by the total volume V and the total number of lipids N of the large system, the free energy per lipid of the bilayer, f_A, and the free energy of pure solvent, $f_s = (\phi_0/V_{sol})\ln(\phi_0/V_{sol})$, where V_s is the volume of the solvent and ϕ_0 is the bulk solvent volume fraction

$$F = F_{box} + F_{out} = Vf_s + Nf_A \quad (3)$$

The free energy per lipid difference due to the insertion of an NP (Fig. 2C) yields the form

$$\Delta F = F_{box} - Nf_A - (V_{box} - V_{obj})f_s \quad (4)$$

where N is the equilibrium number of lipids in the box, V_{box} is the volume of the box, and V_{obj} is the volume of part of the NP inside the box. The reference state for free energy difference was chosen to be the energy of unperturbed bilayer (zero energy in Fig. 3), whereas in Fig. 2, the reference state was the energy of an NP inserted in the bilayer.

Lipid molecules and solutions

All phospholipid molecules were purchased from Avanti Polar Lipids. To prepare the lipid solutions, 20 mg of DMPC was dissolved in 1 ml of squalene (Sigma) with 1% NBD fluorescence–labeled lipids [DPPE-NBD (ammonium salt)]. The electrolyte for electrophysiological measurements consisted of 100 mM NaCl (Sigma-Aldrich) in Milli-Q water. All experiments were conducted at 30°C, where the lipid bilayer was in a fluid phase.

Microfluidics

Microchannels with rectangular cross sections were fabricated using typical soft lithography protocols. Channel dimensions were 300 μm in width and 140 μm in height. The device was molded in SYLGARD 184 (Dow Corning) from an SU-8 photoresist structure on a silicon wafer. The surface of the SYLGARD 184 device was exposed to oxygen plasma (Diener electronic GmbH) and sealed with a plasma-treated glass cover slide. The sealed device was rendered hydrophilic by heating it to 135°C overnight. The liquids were dispensed from syringes (Hamilton Bonaduz AG), which were connected to the microfluidic device by tubing. Custom-made, computer-controlled syringe pumps were used to control the injection of the water and the oil phase. For the fluorescence

microscopy experiments, a commercial micro–particle image velocimetry setup from LaVision was used, with an illumination wavelength of 473 nm and a sensitive CCD (charge-coupled device) camera (Imager pro X).

Patch clamping

Ag/AgCl electrodes were prepared by inserting a silver chloride wire into a borosilicate glass pipette (outer diameter, 1.5 mm; inner diameter, 0.86 mm; Sutter) containing an electrolyte agarose solution. Lipid membrane capacitance was measured using the LockIn function provided by the patch clamp amplifier EPC 10 USB (HEKA Electronics). A 10-mV sinusoidal wave, with a frequency of 20 kHz, was used as the excitation signal. The electrodes were carefully introduced into the aqueous compartment of the SYLGARD 184 device using a micromanipulator.

Nanoparticles

AuNPs were synthesized from the one-step process described by Zheng *et al.* (*57*). These NPs were composed of a gold core (2, 4, or 6 nm) and coated with a dense monolayer of 1-dodecanethiol with a length of 1.6 nm, as described in detail by Donnio *et al.* (*58*). These AuNPs have been characterized in detail by Mancini *et al.* (*59*) using ultrafast small-angle electron diffraction. Transmission electron microscopy analysis showed a size dispersion of around ±0.5 nm for the used NPs with average diameters of 2, 4, and 6 nm. To disperse these particles in an aqueous phase, we added a mixture of NPs and DMPC lipids on top of the aqueous phase. Subsequently, the system was sonicated for a few days. The formation of a stable dispersion of single NPs into the aqueous phase was confirmed by dynamic light scattering and zeta potential analysis (Supplementary Materials).

SUPPLEMENTARY MATERIALS

Supplementary material for this article is available at http://advances.sciencemag.org/cgi/content/full/2/11/e1600261/DC1

Proofs of lipid exchange after NP insertion

fig. S1. Fluorescence micrograph showing that lipids from the NP coating go into the bilayer upon translocation.

fig. S2. Fluorescence microscopy time series.

fig. S3. The three water droplets, described in this section, are observed under epifluorescence microscopy.

fig. S4. Hydrodynamic diameter measurements from dynamic light scattering technique.

fig. S5. Schematic view of 6-nm dodecanethiol-capped AuNPs.

REFERENCES AND NOTES

1. V. Mailänder, K. Landfester, Interaction of nanoparticles with cells. *Biomacromolecules* **10**, 2379–2400 (2009).
2. J. Lin, H. Zhang, Z. Chen, Y. Zheng, Penetration of lipid membranes by gold nanoparticles: Insights into cellular uptake, cytotoxicity, and their relationship. *ACS Nano* **4**, 5421–5429 (2010).
3. H. Schatten, Ed., *Scanning Electron Microscopy for the Life Sciences* (Cambridge Univ. Press, 2012).
4. B. Korzeniowska, R. Nooney, D. Wencel, C. McDonagh, Silica nanoparticles for cell imaging and intracellular sensing. *Nanotechnology* **24**, 442002 (2013).
5. Y. Pan, X. Du, F. Zhao, B. Xu, Magnetic nanoparticles for the manipulation of proteins and cells. *Chem. Soc. Rev.* **41**, 2912–2942 (2012).
6. V. K. Varadan, L. Chen, J. Xie, *Nanomedicine: Design and Applications of Magnetic Nanomaterials, Nanosensors and Nanosystems* (John Wiley & Sons, 2008).
7. J. Choi, N. Sun, in *Biomedical Engineering—From Theory to Applications*, R. Fazel, Ed. (InTech, 2011).
8. G. L. Prasad, *Safety of Nanoparticles*, T. J. Webster, Ed. (Nanostructure Science and Technology, Springer, 2009), pp. 89–109.
9. Y. Li, T.-y. Lin, Y. Luo, Q. Liu, W. Xiao, W. Guo, D. Lac, H. Zhang, C. Feng, S. Wachsmann-Hogiu, J. H. Walton, S. R. Cherry, D. J. Rowland, D. Kukis, C. Pan, K. S. Lam, A smart and versatile theranostic nanomedicine platform based on nanoporphyrin. *Nat. Commun.* **5**, 4712 (2014).
10. J. H. Kang, M. Super, C. W. Yung, R. M. Cooper, K. Domansky, A. R. Graveline, T. Mammoto, J. B. Berthet, H. Tobin, M. J. Cartwright, A. L. Watters, M. Rottman, A. Waterhouse, A. Mammoto, N. Gamini, M. J. Rodas, A. Kole, A. Jiang, T. M. Valentin, A. Diaz, K. Takahashi, D. E. Ingber, An extracorporeal blood-cleansing device for sepsis therapy. *Nat. Med.* **20**, 1211–1216 (2014).
11. H. J. Johnston, G. Hutchison, F. M. Christensen, S. Peters, S. Hankin, V. Stone, A review of the in vivo and in vitro toxicity of silver and gold particulates: Particle attributes and biological mechanisms responsible for the observed toxicity. *Crit. Rev. Toxicol.* **40**, 328–346 (2010).
12. C. Freese, C. Uboldi, M. I. Gibson, R. E. Unger, B. B. Weksler, I. A. Romero, P.-O. Couraud, C. J. Kirkpatrick, Uptake and cytotoxicity of citrate-coated gold nanospheres: Comparative studies on human endothelial and epithelial cells. *Part. Fibre Toxicol.* **9**, 23 (2012).
13. A. M. Alkilany, C. J. Murphy, Toxicity and cellular uptake of gold nanoparticles: What we have learned so far? *J. Nanopart. Res.* **12**, 2313–2333 (2010).
14. I. M. M. Paino, V. S. Marangoni, R. d. C. S. de Oliveira, L. M. G. Antunes, V. Zucolotto, Cyto and genotoxicity of gold nanoparticles in human hepatocellular carcinoma and peripheral blood mononuclear cells. *Toxicol. Lett.* **215**, 119–125 (2012).
15. R. Coradeghini, S. Gioria, C. P. Garca, P. Nativo, F. Franchini, D. Gilliland, J. Ponti, F. Rossi, Size-dependent toxicity and cell interaction mechanisms of gold nanoparticles on mouse fibroblasts. *Toxicol. Lett.* **217**, 205–216 (2013).
16. L. Shang, K. Nienhaus, G. U. Nienhaus, Engineered nanoparticles interacting with cells: Size matters. *J. Nanobiotechnol.* **12**, 5 (2014).
17. D. F. Moyano, M. Goldsmith, D. J. Solfiell, D. Landesman-Milo, O. R. Miranda, D. Peer, V. M. Rotello, Nanoparticle hydrophobicity dictates immune response. *J. Am. Chem. Soc.* **134**, 3965–3967 (2012).
18. A. Verma, O. Uzun, Y. Hu, Y. Hu, H.-S. Han, N. Watson, S. Chen, D. J. Irvine, F. Stellacci, Surface-structure-regulated cell-membrane penetration by monolayer-protected nanoparticles. *Nat. Mater.* **7**, 588–595 (2008).
19. A. Verma, F. Stellacci, Effect of surface properties on nanoparticle–cell interactions. *Small* **6**, 12–21 (2010).
20. Z. Chu, S. Zhang, B. Zhang, C. Zhang, C.-Y. Fang, I. Rehor, P. Cigler, H.-C. Chang, G. Lin, R. Liu, Q. Li, Unambiguous observation of shape effects on cellular fate of nanoparticles. *Sci. Rep.* **4**, 4495 (2014).
21. B. Jing, Y. Zhu, Disruption of supported lipid bilayers by semihydrophobic nanoparticles. *J. Am. Chem. Soc.* **133**, 10983–10989 (2011).
22. B. Jing, R. C. T. Abot, Y. Zhu, Semihydrophobic nanoparticle-induced disruption of supported lipid bilayers: Specific ion effect. *J. Phys. Chem. B* **118**, 13175–13182 (2014).
23. C. L. Ting, Z.-G. Wang, Interactions of a charged nanoparticle with a lipid membrane: Implications for gene delivery. *Biophys. J.* **100**, 1288–1297 (2011).
24. J. Lin, A. Alexander-Katz, Cell membranes open "doors" for cationic nanoparticles/biomolecules: Insights into uptake kinetics. *ACS Nano* **7**, 10799–10808 (2013).
25. V. V. Ginzburg, S. Balijepalli, Modeling the thermodynamics of the interaction of nanoparticles with cell membranes. *Nano Lett.* **7**, 3716–3722 (2007).
26. G. J. Doherty, H. T. McMahon, Mechanisms of endocytosis. *Annu. Rev. Biochem.* **78**, 857–902 (2009).
27. H. T. McMahon, E. Boucrot, Molecular mechanism and physiological functions of clathrin-mediated endocytosis. *Nat. Rev. Mol. Cell Biol.* **12**, 517–533 (2011).
28. J. Liu, Y. Sun, D. G. Drubin, G. F. Oster, The mechanochemistry of endocytosis. *PLOS Biol.* **7**, e1000204 (2009).
29. M. Orsi, J. W. Essex, Permeability of drugs and hormones through a lipid bilayer: Insights from dual-resolution molecular dynamics. *Soft Matter* **6**, 3797–3808 (2010).
30. S. Paula, A. G. Volkov, A. N. Van Hoek, T. H. Haines, D. W. Deamer, Permeation of protons, potassium ions, and small polar molecules through phospholipid bilayers as a function of membrane thickness. *Biophys. J.* **70**, 339–348 (1996).
31. D. Bedrov, G. D. Smith, H. Davande, L. Li, Passive transport of C_{60} fullerenes through a lipid membrane: A molecular dynamics simulation study. *J. Phys. Chem. B* **112**, 2078–2084 (2008).
32. R. Qiao, A. P. Roberts, A. S. Mount, S. J. Klaine, P. C. Ke, Translocation of C_{60} and its derivatives across a lipid bilayer. *Nano Lett.* **7**, 614–619 (2007).
33. C. Bonnaud, C. A. Monnier, D. Demurtas, C. Jud, D. Vanhecke, X. Montet, R. Hovius, M. Lattuada, B. Rothen-Rutishauser, A. Petri-Fink, Insertion of nanoparticle clusters into vesicle bilayers. *ACS Nano* **8**, 3451–3460 (2014).
34. Y. Li, X. Chen, N. Gu, Computational investigation of interaction between nanoparticles and membranes: Hydrophobic/hydrophilic effect. *J. Phys. Chem. B* **112**, 16647–16653 (2008).
35. K. Yang, Y.-Q. Ma, Computer simulation of the translocation of nanoparticles with different shapes across a lipid bilayer. *Nat. Nanotechnol.* **5**, 579–583 (2010).
36. H.-m. Ding, W.-d. Tian, Y.-q. Ma, Designing nanoparticle translocation through membranes by computer simulations. *ACS Nano* **6**, 1230–1238 (2012).

37. A. Davies, D. J. Lewis, S. P. Watson, S. G. Thomas, Z. Pikramenou, pH-controlled delivery of luminescent europium coated nanoparticles into platelets. *Proc. Natl. Acad. Sci. U.S.A.* **109**, 1862–1867 (2012).
38. R. C. Van Lehn, P. U. Atukorale, R. P. Carney, Y.-S. Yang, F. Stellacci, D. J. Irvine, A. Alexander-Katz, Effect of particle diameter and surface composition on the spontaneous fusion of monolayer-protected gold nanoparticles with lipid bilayers. *Nano Lett.* **13**, 4060–4067 (2013).
39. R. C. Van Lehn, M. Ricci, P. H. J. Silva, P. Andreozzi, J. Reguera, K. Voïtchovsky, F. Stellacci, A. Alexander-Katz, Lipid tail protrusions mediate the insertion of nanoparticles into model cell membranes. *Nat. Commun.* **5**, 4482 (2014).
40. Y. Li, X. Li, Z. Li, H. Gao, Surface-structure-regulated penetration of nanoparticles across a cell membrane. *Nanoscale* **4**, 3768–3775 (2012).
41. A. Ben-Shaul, I. Szleifer, W. M. Gelbart, Chain organization and thermodynamics in micelles and bilayers. I. Theory. *J. Chem. Phys.* **83**, 3597–3611 (1985).
42. I. Szleifer, A. Ben-Shaul, W. M. Gelbart, Chain statistics in micelles and bilayers: Effects of surface roughness and internal energy. *J. Chem. Phys.* **85**, 5345–5359 (1986).
43. S. Pogodin, V. A. Baulin, Coarse-grained models of phospholipid membranes within the single chain mean field theory. *Soft Matter* **6**, 2216–2226 (2010).
44. A. Carré, K. L. Mittal, Eds., *Superhydrophobic Surfaces* (VSP, 2009).
45. G. Decher, J. B. Schlenoff, Eds., *Multilayer Thin Films: Sequential Assembly of Nanocomposite Materials* (Wiley-VCH, ed. 2, 2012).
46. S. Pogodin, V. A. Baulin, Can a carbon nanotube pierce through a phospholipid bilayer? *ACS Nano* **4**, 5293–5300 (2010).
47. S. Pogodin, V. A. Baulin, Equilibrium insertion of nanoscale objects into phospholipid bilayers. *Curr. Nanosci.* **7**, 721–726 (2011).
48. S. Pogodin, N. K. H. Slater, V. A. Baulin, Surface patterning of carbon nanotubes can enhance their penetration through a phospholipid bilayer. *ACS Nano* **5**, 1141–1146 (2011).
49. L. D. Mosgaard, T. Heimburg, Lipid ion channels and the role of proteins. *Acc. Chem. Res.* **46**, 2966–2976 (2013).
50. K. Funakoshi, H. Suzuki, S. Takeuchi, Lipid bilayer formation by contacting monolayers in a microfluidic device for membrane protein analysis. *Anal. Chem.* **78**, 8169–8174 (2006).
51. H. Bayley, B. Cronin, A. Heron, M. A. Holden, W. L. Hwang, R. Syeda, J. Thompson, M. Wallace, Droplet interface bilayers. *Mol. BioSyst.* **4**, 1191–1208 (2008).
52. S. Thutupalli, J.-B. Fleury, A. Steinberger, S. Herminghaus, R. Seemann, Why can artificial membranes be fabricated so rapidly in microfluidics? *Chem. Commun.* **49**, 1443–1445 (2013).
53. J. N. Vargas, R. Seemann, J.-B. Fleury, Fast membrane hemifusion *via* dewetting between lipid bilayers. *Soft Matter* **10**, 9293–9299 (2014).
54. R. P. Carney, Y. Astier, T. M. Carney, K. Voïtchovsky, P. H. Jacob Silva, F. Stellacci, Electrical method to quantify nanoparticle interaction with lipid bilayers. *ACS Nano* **7**, 932–942 (2013).
55. H. Fan, K. Yang, D. M. Boye, T. Sigmon, K. J. Malloy, H. Xu, G. P. López, C. J. Brinker, Self-assembly of ordered, robust, three-dimensional gold nanocrystal/silica arrays. *Science* **304**, 567–571 (2004).
56. Y. Tu, M. Lv, P. Xiu, T. Huynh, M. Zhang, M. Castelli, Z. Liu, Q. Huang, C. Fan, H. Fang, R. Zhou, Destructive extraction of phospholipids from *Escherichia coli* membranes by graphene nanosheets. *Nat. Nanotechnol.* **8**, 594–601 (2013).
57. N. Zheng, J. Fan, G. D. Stucky, One-step one-phase synthesis of monodisperse noble-metallic nanoparticles and their colloidal crystals. *J. Am. Chem. Soc.* **128**, 6550–6551 (2006).
58. B. Donnio, P. García-Vázquez, J.-L. Gallani, D. Guillon, E. Terazzi, Dendronized ferromagnetic gold nanoparticles self-organized in a thermotropic cubic phase. *Adv. Mater.* **19**, 3534–3539 (2007).
59. G. F. Mancini, T. Latychevskaia, F. Pennacchio, J. Reguera, F. Stellacci, F. Carbone, Order/disorder dynamics in a dodecanethiol-capped gold nanoparticles supracrystal by small-angle ultrafast electron diffraction. *Nano Lett.* **16**, 2705–2713 (2016).

Acknowledgments: We are grateful to M. Werner and E. Ivanova for the numerous discussions and comments. **Funding:** V.A.B. and Y.G. acknowledge funding from Marie Curie Actions under European Union 7th Framework Programme (FP7) Initial Training Network SNAL 608184. J.B.F. and R.S. acknowledge funding from SFB 1027 (B4). **Author contributions:** E.T. synthesized and characterized the nanoparticles; J.B.F. designed and performed the experiments; Y.G. and V.A.B. developed the theoretical model and performed the calculations; Y.G., R.S., J.B.F., and V.A.B. analyzed the data and discussed the results; J.B.F. and V.A.B. designed the research; and Y.G., E.T., R.S., J.B.F., and V.A.B. wrote the paper. **Competing interests:** The authors declare that they have no competing interests. **Data and materials availability:** All data needed to evaluate the conclusions in the paper are present in the paper and/or the Supplementary Materials. Additional data related to this paper may be requested from the authors.

Submitted 8 February 2016
Accepted 29 September 2016
Published 2 November 2016
10.1126/sciadv.1600261

Citation: Y. Guo, E. Terazzi, R. Seemann, J. B. Fleury, V. A. Baulin, Direct proof of spontaneous translocation of lipid-covered hydrophobic nanoparticles through a phospholipid bilayer. *Sci. Adv.* **2**, e1600261 (2016).

ScienceAdvances

Direct proof of spontaneous translocation of lipid-covered hydrophobic nanoparticles through a phospholipid bilayer

Yachong Guo, Emmanuel Terazzi, Ralf Seemann, Jean Baptiste Fleury, and Vladimir A. Baulin

Sci. Adv. **2** (11), e1600261. DOI: 10.1126/sciadv.1600261